Nonlinear optical properties of carbon-black suspensions (ink)

Kamjou Mansour*

Center for Research in Electro-Optics and Lasers, University of Central Florida, Orlando, Florida 32816

M. J. Soileau and E. W. Van Stryland

Center for Research in Electro-Optics and Lasers and Department of Physics and Electrical Engineering, University of Central Florida, Orlando, Florida 32816

Received August 6, 1991; revised manuscript received March 2, 1992

We performed a series of experiments on suspensions of carbon particles in liquids (ink) and carbon particles deposited on glass to determine the mechanisms for the observed optical-limiting behavior. Both materials show reduced transmittance for increasing fluence (energy per unit area). We found that nonlinear scattering dominates the transmissive losses and that the limiting is fluence dependent, so that limiters based on black ink are effective for nanosecond pulses but not for picosecond pulses. Additionally, the nonlinear scattering and the limiting behavior cease after repeated irradiation. For the liquid, flowing eliminates this effect. All the data obtained are consistent with a model of direct heating of the microscopic-sized carbon particles by linear absorption with subsequent optical breakdown initiated by thermally ionized carriers. A simple calculation gives temperatures higher than the sublimation temperature at the onset of limiting. Emission spectra measurements show singly ionized carbon emission lines with a hot blackbody background emission consistent with temperatures of $\simeq$4000 K. A rapid expansion of the microscopic plasmas generated by the breakdown will effectively scatter further input light. Indeed, in time-resolved experiments the trailing portion of the pulse is most heavily scattered. The time-resolved transmittance of a weak cw probe beam also follows the temporal dependence of the singly ionized carbon emission ($\simeq 10^2$ ns). We directly monitored the expansion of the scattering centers by angularly resolving the scattered light for different input fluences and fitting to Mie scattering theory. Since the carbon is black and the microplasmas are initiated by linear absorption, the limiting is extremely broadband. Within the context of this model we discuss the limitations and optimization of ink-based optical limiters.

1. INTRODUCTION

There is considerable interest in the application of the nonlinear optical properties of materials for optical limiting. The ideal optical limiter would have high linear transmittance for low-input-energy laser pulses and low transmittance for input energies above a user-specified value so that the output would become clamped. In addition, this ideal limiter would have rapid response (picoseconds for some applications), broadband response (e.g., the visible spectrum), and a large dynamic range. Here dynamic range is defined as the ratio of the input energy at which the device no longer clamps the output or at which the device itself is irreversibly damaged to the input energy at which the output first becomes clamped. Figure 1 shows the input–output characteristics of such an ideal limiter. Figure 2 shows the input–output characteristics of a 1-cm-thick glass cuvette filled with a carbon-black suspension (CBS), a suspension of carbon-black particles in a mixture of water and ethylene glycol (i.e., diluted black drawing ink) along with a similar curve for an identical cell filled with carbon disulfide, CS_2.[1,2] In our experiments we filtered the suspension through a 0.25-μm filter, and the largest agglomerates seen after drying and measuring with an electron microscope were 0.21 μm, with an individual particle size of $\simeq$35 nm. Later we will see that scattering measurements gave an average size of $\simeq$0.14 μm. For these measurements the input pulses were focused, 20-nsec (FWHM), 1.06-μm, linearly polarized pulses from a Q-switched Nd:YAG laser run at a repetition rate of 1 Hz. The power needed to initiate limiting in a CBS of $\simeq$100 W (energy $\simeq$1 μJ) is compared with kilowatts for CS_2. This low threshold for limiting makes CBS's interesting for a variety of applications.

In this paper we report a comprehensive series of experiments aimed at determining the basic physical mechanisms responsible for the nonlinear response observed in Fig. 2. Our conclusion from the results of these experiments is that the tiny suspended carbon particles are rapidly heated by strong linear absorption, giving rise to thermionic emission, which in the presence of the strong electric field leads to avalanche ionization. The resulting microplasmas then rapidly expand into the surrounding liquid and strongly scatter the incident light for the duration of the existence of the plasma ($\simeq 10^2$ ns). Subsequently, at incident energies well above the threshold for obtaining a clamped output, the heating leads to bubble formation and further scattering that lasts for microseconds. These conclusions imply that the limiting is broadband and depends on fluence (energy per unit area) rather than on irradiance, both of which agree with our observations. In addition, since the carbon particles are ionized (and vaporized) during the process, the suspension must be replenished after each laser exposure, again

0740-3224/92/071100-10$05.00

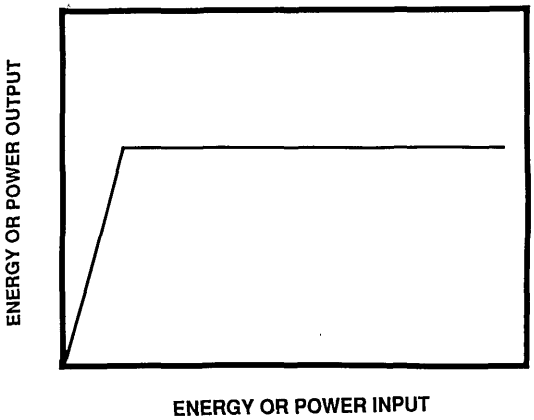

Fig. 1. Power or energy output of an ideal passive optical limiter as a function of the input peak power or energy.

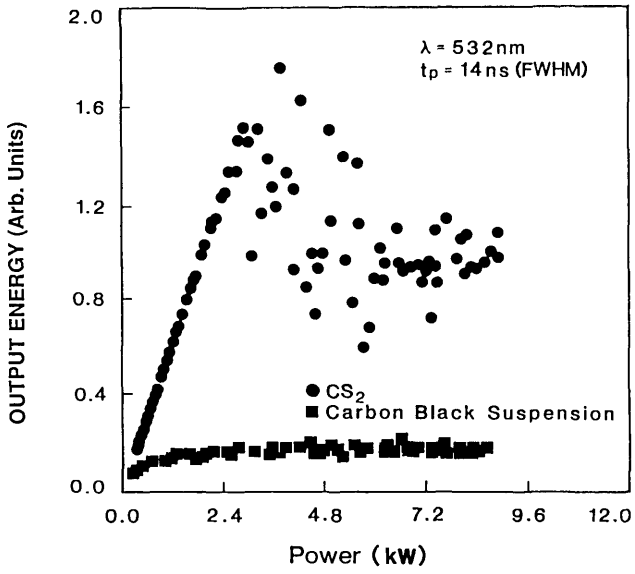

Fig. 2. Energy output for CS_2 and CBS as a function of input peak power for 14-ns (FWHM), 532-nm pulses focused to $w_0 \simeq 3.5$ μm for input powers of 1 to 12 kW.

as observed. The experiments leading to these conclusions and the organization of this paper are briefly outlined below.

In Section 2 we first describe optical limiting experiments on the CBS and on a sample of carbon particles deposited upon glass (CBG) performed at 1.06 and 0.53 μm with both nanosecond and picosecond input pulses. In Section 3 we describe three methods for monitoring the contribution of nonlinear refraction to limiting, all of which showed negative results. In Section 4 we describe the results of an experiment in which we simultaneously monitored transmittance, absorptance, and the fraction of side-scattered light in CBS, and we also describe a similar experiment in CBG in which we measured transmittance and scattering. Time-resolved transmittance measurements using both a single beam and a pulse–probe technique are discussed in Section 5. In Section 6 we show results of emission-spectra measurements, and we time resolve them. The results of these measurements suggest that microplasmas that scatter the incident light are being formed. Growth of these plasmas in size must be the explanation for the observed limiting, since the carbon particles already block some of the transmission by their high linear absorption. In Section 6, therefore, we compare the results of measurements of the angular distribution of the side-scattered light for different fluences with results obtained with theory. This comparison confirms growth of the scattering centers as fluence increases. Finally, in Section 8 we look at limiting geometries for which the sample thickness is large compared with the depth of focus of the input beam (thick-sample geometry), and we show why what is fundamentally a fluence-dependent nonlinearity manifests itself as an energy dependence in this thick-sample geometry.

2. OPTICAL LIMITING

Using a nanosecond Q-switched Nd:YAG laser and a mode-locked picosecond Nd:YAG at 1064 and 532 nm, we examined optical limiting in a CBS and CBG as a function of carbon-black microparticle concentration, input polarization, repetition rate, and beam radius. For 14-ns, 532-nm linearly or circularly polarized laser pulses incident upon a 1-cm-thick sample of CBS with 70% linear transmission at 532 nm, we found that the onset of limiting begins for incident peak powers of the order of 100 W for a tight-focusing limiting geometry, as shown in Fig. 3. However, the output is approximately clamped (i.e., the slope of output versus input becomes small) for incident powers $\gtrsim$160 W. This value (the limiting threshold) is that input power (energy, fluence, or irradiance) at which the linear response line, in a plot of output versus input, intersects the line passing through the "clamped" output. This limiting threshold is approximately 1/24 that for CS_2 ($\simeq$3.8 kW) if the same focusing geometry is used. The reorientational nonlinearity in CS_2 is known to lead to a power-dependent limiting.[3] The lower limiting threshold in CS_2 for 14-ns laser pulses compared with that for single 42-ps pulses ($\simeq$8 kW) possibly results from electrostrictive self-focusing that occurs for the longer pulses with a tight-focusing geometry.[4] Identical focusing geometries were

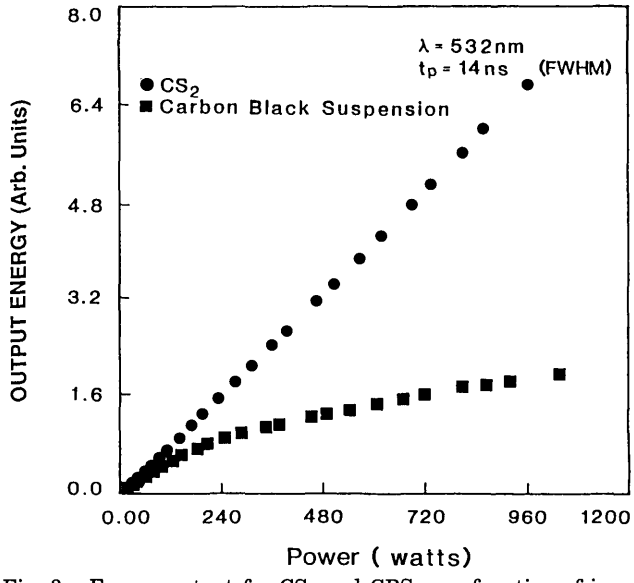

Fig. 3. Energy output for CS_2 and CBS as a function of input peak power for 14-ns (FWHM), 532-nm pulses focused to $w_0 \simeq 3.5$ μm for input powers of 1 to 1000 W.

Table 1. Limiting Thresholds for CBS and CS_2 in a Tight-Focusing Geometry

Material	λ (nm)	w_0 (μm)	t_p (ns)	Power (kW)	Energy (μJ)	Fluence (J/cm^2)
CS_2	532	3.5	14	3.8	57	300
CS_2	532	3.5	0.042	8	0.36	1.9
CS_2	1064	5.1	20	13.5	290	710
CBS	532	3.5	14	0.16	2.4	12
CBS	532	3.5	0.042	30	1.3	6.8
CBS	1064	5.1	20	0.40	8.5	21

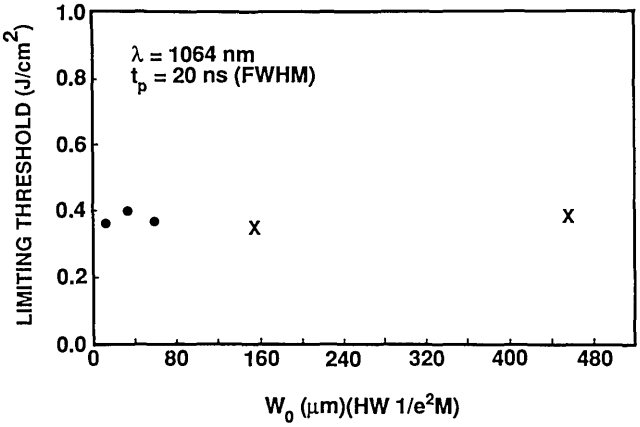

Fig. 4. Limiting threshold fluence as a function of beam radius for 20-ns (FWHM), 1064-nm laser pulses. Circles represent the measured value for a 100-μm-thick flowing jet of CBS with 70% linear transmittance, and ×'s are for a 1-cm-thick sample of CBS with a 70% linear transmittance at 1064 nm (the thin-sample criterion is satisfied).

used in experiments with both the nanosecond and picosecond laser sources. The calculated spot size at focus at 532 nm was $w_0 \simeq 3.5$ μm (half-width at $1/e^2$ maximum in irradiance). Best-form lenses were used for focusing the laser beam in all experiments reported in this paper. We found that for 20-ns, 1064-nm laser pulses focused to $w_0 \simeq 5.1$ μm, a CBS limits the output for an incident power of $\simeq$400 W, which is approximately 1/34 that of the threshold for CS_2 at this wavelength. These results clearly indicate that a CBS is a promising material for optical limiting applications, such as optical sensor protection. However, for single 42-ps, 532-nm laser pulses the limiting occurs for incident peak powers of the order of $\simeq$30 kW at 532 nm if a tight-focusing geometry similar to that used for the nanosecond laser pulse experiment is used. This limiting threshold is nearly four times that for CS_2 ($\simeq$8 kW). These results are summarized in Table 1. We conclude that limiting works well in a CBS for long pulses ($\geq$10 ns) but is less effective for short (picosecond) pulses. We found that for tight-focusing geometries the limiting depends on input energy, whereas for a collimated beam geometry the limiting depends on fluence (J/cm^2). The energies (and fluences) for limiting in a CBS for nanosecond and picosecond pulses are equal to within better than a factor of 2, as may be seen from Table 1. The small difference (picosecond pulses limit at a slightly lower energy) could be due to small geometry differences and self-focusing in the solvent at the high irradiance used for picosecond pulses.

In Section 8 we discuss the reasons for energy-dependent rather than fluence-dependent limiting for thick (tight-focusing) versus thin limiters. For thin limiters (i.e., those in which the beams are well collimated within the length of the sample) we used focal beam radii of 14–454 μm with nanosecond laser pulses incident upon a 100-μm-thick jet of flowing CBS (as in a dye laser) to measure the limiting threshold. The results shown in Fig. 4, along with the picosecond measurements discussed above, demonstrate that the limiting is fluence dependent. These measurements show that the onset of limiting (for collimated beams) occurs at $\simeq$200 mJ/cm^2 for 532-nm, 14-ns (FWHM) pulses (not shown) and at $\simeq$380 mJ/cm^2 for 1064-nm, 20-ns (FWHM) pulses, independent of spot size. Thus optical nonlinearities leading to limiting in a CBS depend on the temporally integrated irradiance (i.e., fluence).

We found that the onset of limiting is independent of the concentration of carbon-black particles. However, samples with a higher concentration of carbon-black particles and, in turn, lower transmittance for low-input-light levels block the output light more effectively at higher incident fluences than do samples with a low concentration of carbon particles. As we discuss below, the attenuation of the output light is dominated by scattering from microplasmas initiated at the positions of the carbon particles. Therefore we should observe more microplasma scattering centers and stronger attenuation for the more highly concentrated samples.

The optical nonlinearities in the solvent make a negligible contribution to the limiting processes in the CBS for nanosecond inputs. However, because of the presence of highly absorbing carbon-black microparticles in the CBS, heat diffusion to the surrounding liquid could lead to thermal nonlinearities in the solvent. We investigated the effects of such nonlinearities and found that the nonlinear index change was $\lesssim 3 \times 10^{-6}$ (see Section 3). This nonlinear index change is too small to have any significant effect on the limiting threshold for a CBS. In addition, we studied the optical-limiting response of CBG. Here, there is no liquid to heat, and we can ignore the thermal nonlinearities of the host medium. We found the optical limiting threshold for CBG to be $\simeq$800 W peak power for 20-ns, 1064-nm laser pulses, as shown in Fig. 5. This limiting

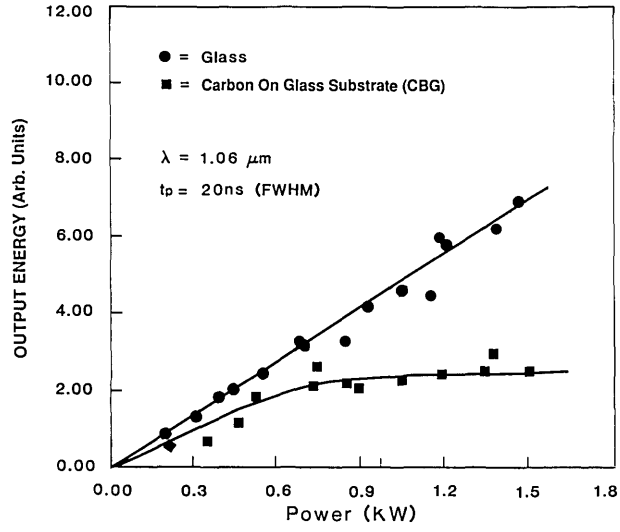

Fig. 5. Energy output for CBG and glass substrate as a function of input peak power for 20-ns (FWHM), 1064-nm pulses focused to $w_0 \simeq 8$ μm. The solid lines are guides for the eye.

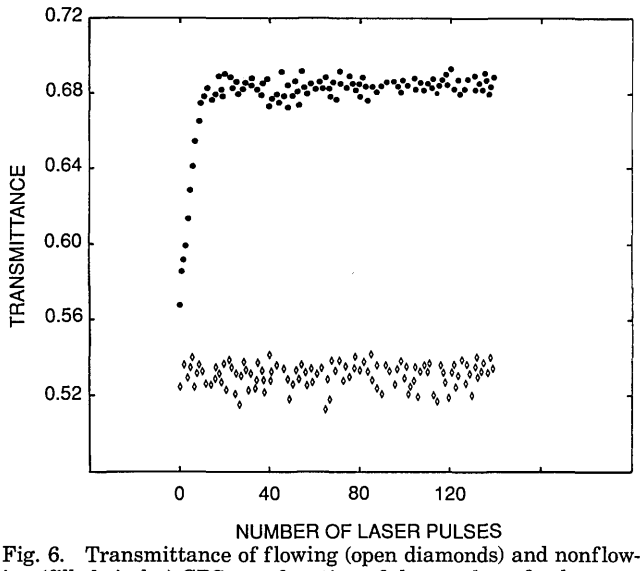

Fig. 6. Transmittance of flowing (open diamonds) and nonflowing (filled circles) CBS as a function of the number of pulses at a repetition rate of 10 Hz with a beam radius of 330 μm and input energy of 2.8 mJ for 20-ns (FWHM), 1064-nm laser pulses. The maximum transmittance of $\simeq$70% is from the finite aperture of the detector in this experiment.

threshold is only twice that of the CBS. This factor-of-2 difference may result from the different particle sizes in these samples. Whereas CBS has an average particle size of $\simeq$0.14 μm, the toner particles used for CBG have an average size of $\simeq$5 μm. Thus for the same input fluence the temperature rise is smaller in the larger particles, and this leads to a higher threshold.[4]

We observed that for a pulse repetition frequency $\gtrsim$2 Hz the limiting effect diminished after a few laser firings. This is illustrated in Fig. 6 for a 10-Hz pulse repetition frequency. The magnitude of this effect depends on the beam radius and input energy. In addition, for CBG, if we did not translate the sample after each laser firing for inputs above the limiting threshold, limiting ceased for subsequent pulses. Examination of the glass slide showed that the particles were removed from the surface after irradiation. Flowing the liquid at a rate sufficient to replenish the CBS between laser firings removes the apparent dependence on pulse repetition frequency.

To understand the optical nonlinearities leading to the observed nonlinear transmittance, we investigated nonlinear refraction (self-focusing or defocusing), nonlinear absorption, nonlinear scattering, and combinations of these mechanisms.

3. NONLINEAR REFRACTION

The contribution of nonlinear refraction in a CBS was studied by using three different techniques: beam distortion,[4,5] measurement of the transmitted on-axis irradiance,[6,7] and the Z-scan method.[8] These techniques allowed us to investigate the contributions of phase distortion from a thermo-optic effect, electrostriction, or any other nonlinear refractive mechanism. Using the beam-distortion measurement, we monitored the far-field spatial transmitted beam profiles of the TEM_{00} Gaussian input pulses at 532 and 1064 nm from a Nd:YAG Q-switched laser as a function of incident irradiance. The beam-distortion measurements indicate that the contribution of nonlinear refraction to optical limiting is small. We estimated the upper limit of the nonlinear refractive index n_2 to be $\simeq 4.6 \times 10^{-12}$ esu at 532 nm. This value was calculated with the assumption that the maximum phase distortion was $<0.3\lambda$ (the sensitivity limit of this technique) for both wavelengths, even at inputs 20 times the optical limiting threshold in a CBS. By using the more sensitive Z-scan technique with wave-front distortion sensitivity $\simeq\lambda/25$ for our laser system, we found that the estimated value of n_2 for CBS was $\simeq 8 \pm 5 \times 10^{-12}$ esu at 532 nm. The positive sign eliminates the possibility of thermal defocusing. If we compare the n_2 of CBS with that of the solvent calculated by Marburger's equation[9] for catastrophic self-focusing, we find that the values agree to within the range of error; thus the measured n_2 value is that of the solvent. This clearly indicates that for intensities for which limiting is observed in CBS, the contribution of nonlinear refraction is negligible. This point also was confirmed by the on-axis transmittance measurement, in which we measured the limiting threshold for CBS with or without an aperture in front of the transmission detector and observed no change in limiting threshold. Note that these measurements also indicate that the small-angle forward scattering is always smaller than the transmitted beam.

4. SIMULTANEOUS MEASUREMENT OF TRANSMITTANCE, ABSORPTANCE, AND SCATTERING

Figure 7 shows the experimental setup used for the simultaneous measurement of absorptance (A), the fraction of side-scattered light (S), and the transmittance (T) in a CBS for nanosecond laser pulses at 532 and 1064 nm. This experiment was performed with a well-collimated beam within the length of the sample. The absorptance signal was obtained by placing a piezoelectric transducer at the bottom of the CBS-filled cell. The gated signal voltage from this transducer (with a peak-and-hold circuit) is directly proportional to the absorbed energy.[10] Figure 8 shows the results of these measurements as a function of incident fluence at 1.06 μm. Data taken at 532 μm show qualitatively identical results. The data shown are for inputs near the threshold for limiting, so that only a small change in transmittance is seen. The transmittance data are absolutely calibrated, whereas the absorptance and scattering fraction are arbitrarily scaled (i.e., $A + S + T \neq 1$ in this figure). The deviation from a horizontal straight line indicates nonlinear behavior for all three signals.

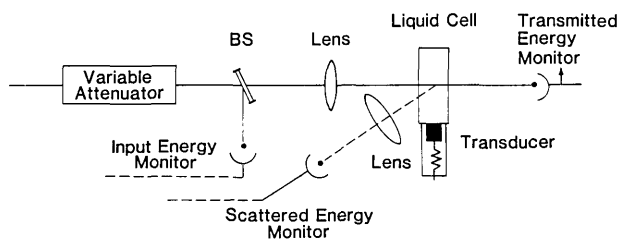

Fig. 7. Schematic diagram for simultaneous measurements of transmittance, absorptance, and the fraction of side-scattered light. BS, beam splitter.

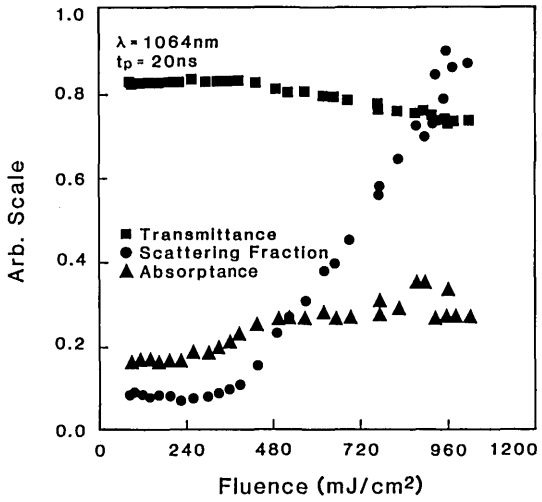

Fig. 8. Transmittance, absorptance, and scattering fraction as a function of incident fluence for 1064-nm, 20-ns (FWHM) pulses focused to $w_0 \simeq 156$ μm for incident fluences of 0.08 to 1 J/cm^2.

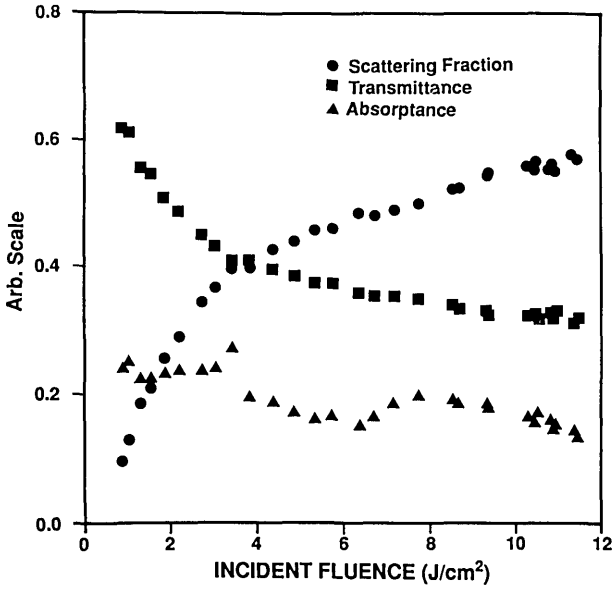

Fig. 9. Transmittance, absorptance, and scattering fraction as a function of incident fluence for 1064-nm, 20-ns (FWHM) pulses focused to $w_0 \simeq 156$ μm for incident fluences of 1 to 12 J/cm^2.

We found that for fluences above the onset of a change of transmittance (i.e., $\simeq$200 mJ/cm^2 for 14 ns, 532 nm and 380 mJ/cm^2 for 20 ns, 1064 nm), there is a strong increase in the fraction of side-scattered light as well as an increase in the absorptance. The absorptance levels fall off for higher fluences. In addition, we found that the trend of increased side-scattered fraction continues for input fluences even 50 times the threshold, as is shown in Fig. 9. These data indicate that for relatively low fluence levels the material changes from a linear absorber to a nonlinear scatterer.

The strong nonlinear scattering is illustrated best in Fig. 10, which is a photograph of the 532-nm side-scattered light at low [Fig. 10(a)] and high [Fig. 10(b)] fluences. Note that at the high fluence level the input never reaches the back of the cell. That light from plasma emission is overwhelmed by side-scattered laser light was quantitatively verified in experiments on the angular scattering profile; these are discussed in Section 7. Only at 1.06 μm could we see the plasma emission in a darkened room after our eyes had adapted to the darkness.

We repeated the measurement of transmittance T and side-scattered fraction S for CBG at 1.06 μm and found that, as the transmittance decreased for fluences $\gtrsim$1 J/cm^2, the side-scattered fraction rapidly increased, as for a CBS, again indicating similar mechanisms for the two materials, independent of surroundings. We were unable to perform the photoacoustic experiment to monitor the absorption because the sample had to be moved after each irradiation, changing the photoacoustic signal in an unpredictable fashion.

5. TIME-RESOLVED TRANSMISSION

We performed time-resolved transmission measurements for the 14-ns, 532-nm laser pulses in a CBS. For fluences below the onset of limiting, the material behaves linearly, and the shapes of input and output pulses are the same, as is shown in Fig. 11. However, for fluences above limiting, we observed that a transmittance cutoff occurs within the duration of the pulse and that latter portions of the pulse are strongly attenuated. This is shown in Fig. 11(b), for which the input reference was attenuated by a factor of 10 with respect to the transmitted pulse, which now appears shifted toward early times because of the truncation. These results are reminiscent of those of laser-induced breakdown experiments.[11,12] The results of this experiment and those described in the previous sections indicate that the physical mechanisms leading to the truncation of

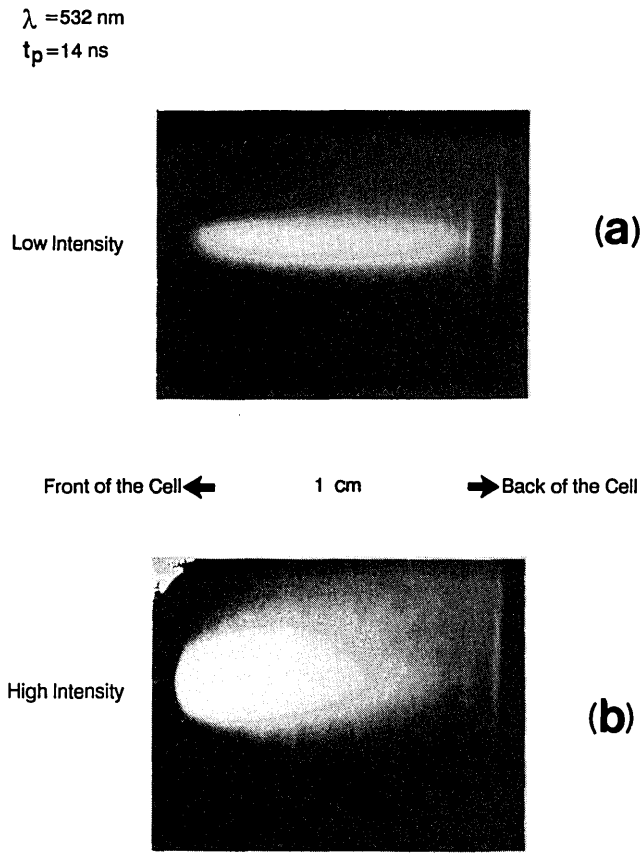

Fig. 10. Photographs of side-scattered 532-nm light from a 1-cm cuvette of CBS for (a) low and (b) high incident intensities (fluences).

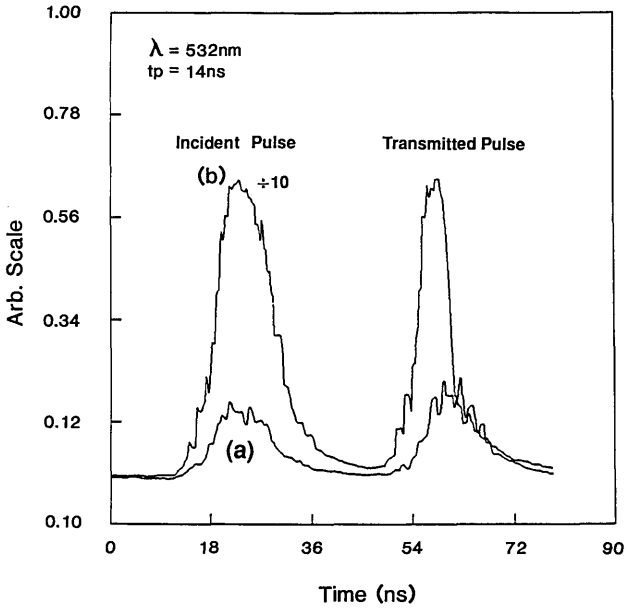

Fig. 11. Temporal profiles of the incident and transmitted 532-nm, 14-ns (FWHM) laser pulses. (a) Incident and transmitted pulses for fluences of ≈100 mJ/cm^2 (below threshold). (b) Incident (attenuated by a factor of 10) and transmitted pulses for a fluence of ≈1.1 J/cm^2 (above threshold). The spot size was $w_0 \simeq 250$ μm.

the pulse and subsequent absorption and scattering of the final portion of the pulse may result from the formation and rapid expansion of microplasmas, as occurs in laser-induced breakdown. Before truncation, carbon-black particles linearly absorb the leading edge of the pulse efficiently. The carbon particles are rapidly heated, and the carbon vaporizes and ionizes to form a rapidly expanding microplasma that strongly scatters and absorbs the latter part of the pulse. If microplasmas are formed, we should be able to monitor their emission spectrum and time resolve both their emission and the induced transmittance changes. Such experiments are described in Section 6.

6. EMISSION SPECTRUM AND TEMPORAL DEPENDENCE

We examined the microplasma formation by using spectrally and temporally resolved fluorescence measurements. We monitored the side emission spectrum with a monochromator–fast-photomultiplier system connected to a computer-controlled digitizing oscilloscope. The laser pulses at 1.06 μm were focused into the CBS or onto the CBG, and the side-scattered light was collected onto the entrance slit of the 0.25-m monochromator. The samples were repetitively irradiated at a fixed fluence (the CBG sample was moved after each firing), and the wavelength was scanned. Figure 12 shows spectral data for CBG. Superimposed upon the data is a blackbody spectrum at 4250 K, which is higher than the sublimation temperature of carbon (≈3850 K). Singly ionized carbon emission wavelengths that coincide with emission peaks in the observed spectra are shown. Data for the CBS show qualitatively similar results, except that the frequency range over which data could be taken was significantly reduced by self-absorption and scattering within the CBS.

The temporal dependence at specific wavelengths was monitored by using the same monochromator–fast-photomultiplier combination. Monitoring the emitted light at ≈800 nm, which coincides with a singly ionized carbon emission peak, resulted in the data of Fig. 13 for CBG. Whereas the decay does not fit a single exponential, the emission decays to 1/*e* of its initial value in ≈10^2 ns. This decay time is consistent with previous measurements for the lifetime of ionized carbon.[13,14]

This ≈10^2-ns decay time is also consistent with the results of excitation and probe measurements in which we monitored the change in the transmittance of a cw He–Ne beam as a function of the incident fluence of a 20-ns, 1064-nm excitation pulse. From this measurement, shown in Fig. 14, we found that for the CBS the He–Ne transmission recovers to 50% of the attenuation within ≈100 ns, which is comparable with the emission time of ionized carbon. Figure 15 shows similar results for CBG. However, for CBG at longer times the transmittance actually increases above the original level. This again indicates that the carbon is ionized and vaporized so that it no longer efficiently absorbs or scatters the incoming light. This is not seen in the CBS, since the material is thick and only a small fraction of the carbon is vaporized with a single laser firing. At the very highest fluence levels in the CBS the transmittance does not fully recover to the original level. This may be attributed to another high-

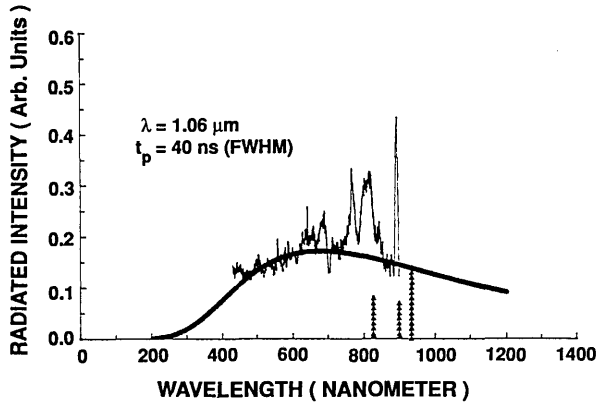

Fig. 12. Spectral emission from carbon particles irradiated by 40-ns, 1.064-μm laser pulses. The triangles show tabulated wavelengths for singly ionized emission lines. The thick solid curve shows the calculated emission for a blackbody source at 4250 K.

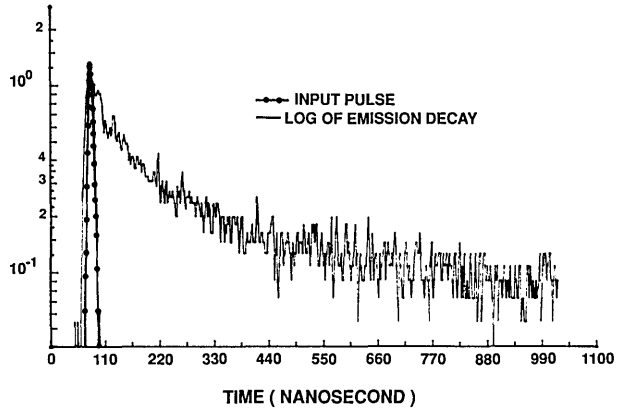

Fig. 13. Semilogarithmic plot of the emission signal at 800 nm as a function of time.

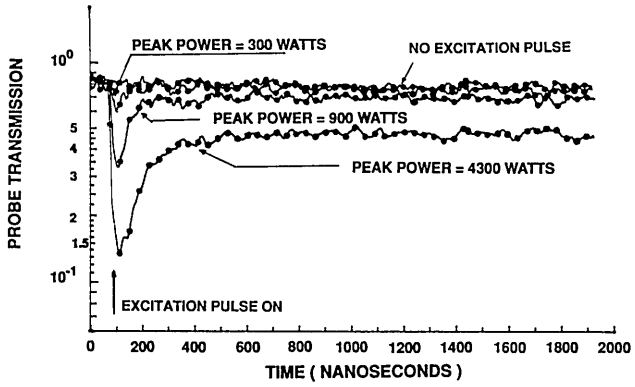

Fig. 14. Semilogarithmic plot of the He–Ne probe-beam transmittance as a function of time for different input powers for 20-ns (FWHM), 1.064-μm excitation pulses for a sample of a CBS with 70% linear transmittance. The dots highlight the digitized curves at specific time intervals.

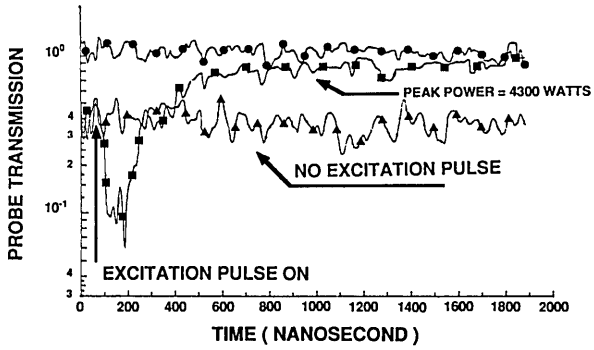

Fig. 15. Semilogarithmic plot of the He–Ne probe-beam transmittance as a function of time for a 4.2-kW, 20-ns (FWHM), 1.064-μm laser pulse for a sample of CBG with 28% linear transmission at 632.8 nm. The dots, triangles, and squares highlight the digitized curves at specific time intervals.

input limiting mechanism, such as vapor formation (i.e., cavitation and bubble formation), which can scatter light for microseconds.[15] Indeed, at high inputs bubbles can be seen in the cell and have been reported by other researchers.[16]

The fact that we see the transmittance of CBG almost completely recover to the uncoated glass slide transmittance within ≈600 ns implies that the carbon particles are removed or destroyed within this time. To be removed the particle velocities would need to be near the speed of sound if we assume velocities perpendicular to the beam. We conclude that the carbon particles are destroyed (vaporized or atomized) in the limiting process. The result is smaller particles (or atoms) much smaller than the wavelength λ, so that they no longer scatter or absorb the light efficiently. This conclusion is consistent with the limiting behavior discussed in Section 2.

7. ANGULAR SCATTERING PROFILE

To study the nonlinear scattering process in this material, we measured the intensity of the scattered light as a function of angle from 20° to 160°, using a 100-μm-thick flowing jet of CBS with nanosecond 532- and 1064-nm laser pulses. Spike filters that transmit only the laser frequency were placed in front of the detectors, as in the other transmittance and scattering experiments. The results of these measurements indicate an increase in the scattered light in the forward direction for fluences for which limiting was observed. The normalized scattered radiation pattern for 1064-nm light is shown in Figs. 16 and 17 for fluences near and four times as high as the limiting threshold, respectively. From these results we determined the average size and the index of refraction of the scattering centers by numerically fitting the experimental results with Mie scattering theory. The best theoretical fits to the experimental results are shown as

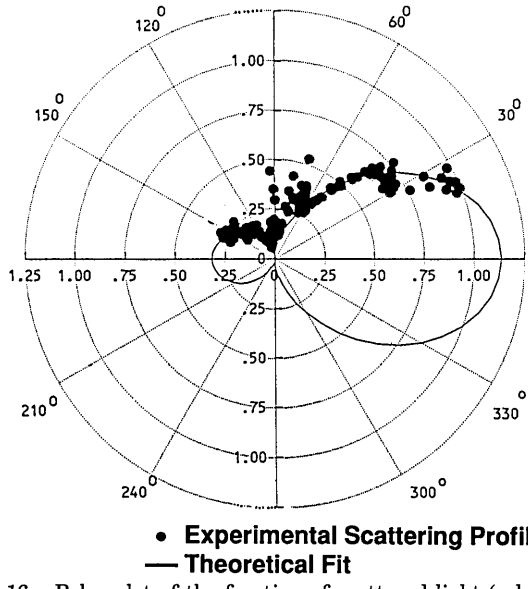

Fig. 16. Polar plot of the fraction of scattered light (arbitrarily scaled) for a CBS for an incident fluence of ≈550 mJ/cm^2 for 20-ns (FWHM), 1064-nm linearly polarized light parallel to the plane of observation. The spot size was $w_0 \simeq 96$ μm. The theoretical fit is based on Mie scattering theory.

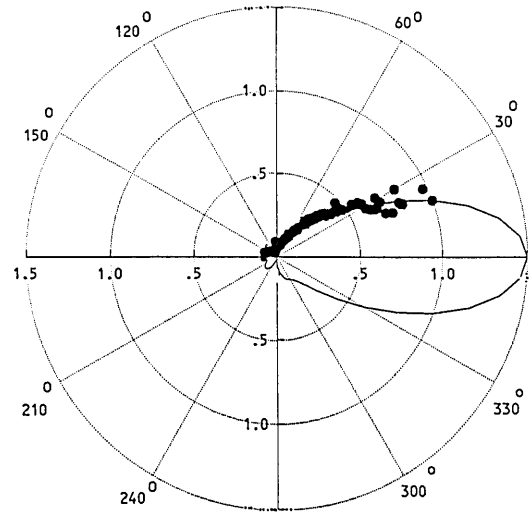

Fig. 17. Polar plot of the fraction of scattered light (arbitrarily scaled) for a CBS for an incident fluence of ≈1.5 J/cm^2 for 20-ns (FWHM), $w_0 \simeq 96$-μm, 1064-nm linearly polarized light parallel to the plane of observation. The theoretical fit is based on Mie scattering theory.

solid lines in Figs. 16 and 17. We found that the average radius of the carbon particles at low input energies is of the order of 0.14 μm with a complex index of refraction $m = 2.16 - 0.77i$ and that the average size of the induced scattering centers (at high input energies) is of the order of 0.40 μm with a complex index of refraction $m = 1.96 - 0.11i$. These results not only indicate that the induced scattering centers are larger by a factor of $\simeq 3$ than the initial particles but also reveal that the optical properties of these centers are different from those of the initial particles. Similar results were observed at 532 nm. Clearly, this measurement integrates the scattering over the entire pulse width during the time the scattering centers are growing. Presumably the average size at the end of the pulse is considerably larger than that measured in these experiments. We attribute the production of the induced scattering centers to the formation and rapid expansion (within the pulse width) of microplasmas initiated by rapid heating and subsequent thermoionization of the carbon particles. The increase in size but decrease in the imaginary part of m (i.e., decrease in absorption) can explain the observed small increase in overall absorptance but large increase in scattering. In particular, the absorption of the particles decreases significantly (i.e., by a factor of $\simeq 7$). Thus the area increases by approximately 3^2, whereas the loss decreases by $\simeq 7$, which is consistent with the observed small increase in absorption.

8. THICK-SAMPLE LIMITING

The experiments described in previous sections that show the fluence dependence of the limiting in CBS were performed with thin-sample geometry, for which the depth of focus of the input beam is larger than the sample thickness. This ensures that the beam is collimated in the sample. We found that the fundamental fluence dependence of limiting in a CBS (or CBG) manifests itself quite differently if the focusing geometry is changed so that the sample is much thicker than the beam depth of focus (i.e., thick-sample or tight-focus geometry). This is expected for a fluence-dependent nonlinearity, as is described below. It is analogous to the irradiance-dependent two-photon absorption (2PA) that appears as a power dependence in tight-focusing geometries.

In this experiment the input beam at 532 nm was focused into the CBS sample with a linear transmittance of 60% by using one of three lenses with focal lengths of 51, 25.5, and 10 mm. The depth of focus for all three lenses is much less than the cell thickness of 1 cm. The spot size at the input lens position was $w_0 \simeq 0.207$ cm half-width at $1/e^2$ maximum at 0.53 μm. The input (and output) energy was monitored by a 1-cm-aperture, uniform-response p-i-n photodiode to collect all of the transmitted beam for each of the input lenses. The output energy versus input energy was recorded for one input lens focal length, and then the input lens was changed. This was repeated for all three input lens focal lengths.

Figure 18 shows the data plotted as transmittance (output divided by input) versus input energy. The downward slope shows the limiting behavior. We know that all the light was collected because the linear transmittance (output energy divided by input energy for low input energy) is independent of the lens used and is approximately equal to the linear transmittance of the 1-cm-thick cell of $T \simeq 0.6$. The important point to be made from these data is that the curves for all three lenses are nearly the same. There is a deviation of the data for the most tightly focused lens (10-mm focal length) at high input energies for which the limiting becomes less efficient (not shown), but this deviation is much smaller than that expected for a fluence-dependent nonlinearity.

The following argument shows how a fluence-dependent nonlinearity (or an irradiance-dependent nonlinearity, such as 2PA) can behave as an energy-dependent (or power-dependent in the case of 2PA) nonlinearity for a thick-sample geometry.

The depth of focus z_0 of a lens is given by

$$z_0 = \frac{\pi w_0^2}{\lambda}, \tag{1}$$

where w_0 is the beam radius at the focus of the lens (half-width at $1/e^2$ maximum). The area of the beam is given by

$$A = \frac{\pi w_0^2}{2}. \tag{2}$$

If the nonlinear interaction is fluence dependent, the transmission change will, to some approximation, be proportional to the product of the fluence and the effective interaction length L_{eff}. For a short cell L_{eff} is the sample thickness, and the nonlinear change in transmittance is fluence dependent. However, for the thick cell, the interaction length can be given approximately by z_0. Thus the change in transmittance (ΔT) is

$$\Delta T \propto F z_0 = \frac{\text{Energy}}{A} z_0 = \text{Energy} \frac{2}{\pi w_0^2} \frac{\pi w_0^2}{\lambda} = \text{Energy} \frac{2}{\lambda}. \tag{3}$$

So now the nonlinear change in transmittance appears to be energy dependent and is independent of the beam size

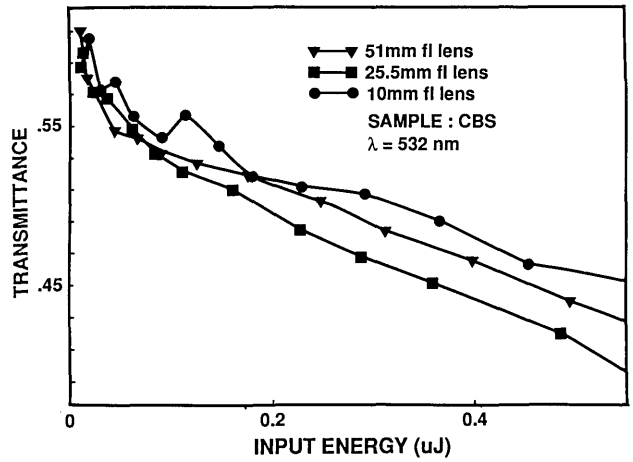

Fig. 18. Plot of transmittance of a 1-cm-thick sample of CBS with $\simeq 60\%$ linear transmittance at 532 nm as a function of input energy for a thick limiter for 5-ns (FWHM) laser pulses for input lenses with focal lengths of 51, 25.5, and 10 mm.

at focus. That is, ΔT is independent of both the focal length of the input lens and its f-number, and this is what our experimental results show. In addition to these focal considerations, the effects of lens aberrations may also be contributing since we are using short-focal-length lenses and small f-numbers.[17] However, we cannot easily determine how large such aberration effects are.

This result may be clearer in the case of 2PA, for which the nonlinear equations are well defined and the irradiance change dI with depth in the sample dz is

$$\frac{dI}{I} = -\beta I dz, \tag{4}$$

where β is the 2PA coefficient. This means that the change in transmittance is approximately

$$\Delta T = \frac{\Delta I}{I} = -\beta I L_{\text{eff}}, \tag{5}$$

where L_{eff} is the effective interaction length. For a thick cell the inverse area dependence of the irradiance cancels the area dependence of $L_{\text{eff}} \simeq z_0$, which leaves ΔT power dependent.

Our conclusion from these data is that extremely tight focusing is not helpful in lowering the threshold and may indeed be detrimental to the performance. However, focusing is necessary for obtaining sufficient fluence to ionize the carbon particles in CBS. A compromise between these requirements is needed.

9. CONCLUSION

We conclude that the dominant nonlinearity leading to limiting in both carbon black suspension and carbon deposited on glass is nonlinear scattering and that the mechanism for this nonlinearity is rapid heating of carbon particles and their subsequent vaporization and ionization, which lead to the formation of rapidly expanding microplasmas.

We can estimate the temperature rise of the carbon particles at the limiting threshold if we are given the laser-beam parameters and the optical properties of carbon black. Ackerman and Toon[18] give the complex index of refraction of carbon black as $m = 1.96 - 0.66i$, which gives an absorption coefficient of $\alpha \simeq 3 \times 10^4$ cm^{-1}. These values are consistent with our measurements of the Mie-scattered light. Donnet and Voet[19] show that absorption with the different types (sizes, etc.) of carbon particles varies by factors of no more than 2 to 3 and scales linearly with concentration. It is also observed that the optical properties of a carbon-black dispersion in a liquid behave similarly to those of the powder form. This is true since the powder form generally has a void volume of over 90%, so that it may be considered a dispersion in air. This, in turn, implies that the absorption that must be used to calculate a temperature rise for carbon without voids is an order of magnitude larger than the reported value. If we use this higher value of $\alpha \simeq 3 \times 10^5$ cm^{-1} and assume single carbon particles of diameter $\simeq 0.14$ μm, we estimate a temperature increase of approximately 10^4°C with 12-nsec, 20-MW/cm^2 pulses. This is consistent with the temperature experimentally estimated from emission measurements.

The dominant role of nonlinear scattering in this process was shown by simultaneous measurements of transmittance, absorptance, and the fraction of side-scattered light. In addition, nonlinear refraction was shown to be insignificant, and the absorptance changed only by a factor of 2, a change far too small to explain the observed limiting. Measurements on CBG confirmed the role of scattering, independent of the surrounding liquid. How scattering could increase the loss over that from the already highly absorbing carbon-black particles is explained by the growth in size and change of index of refraction of the scattering centers. The angular dependence of the side-scattered-light fit to Mie theory demonstrated this growth. The observed volumetric expansion of the plasma is necessary because the volume percent of carbon is small and the carbon particles are already highly absorbing. In addition, the index changes observed in these experiments are not consistent with either shock waves or bubble formation.

The nature of the scattering centers as ionized particles was confirmed from line emission spectra and time-resolved fluorescence measurements, which were consistent with previous measurements of plasma production with carbon targets.[20] The time-resolved transmittance measurements also showed that the limiting lasted only for the lifetime of the microplasma, which is again consistent with the microplasma scattering model. The role of bubble formation at the onset of limiting was investigated by performing experiments on samples of CBG. The similarity of the results obtained for these samples and those for the liquid suspensions shows that bubbles are not important at or near threshold. However, well above threshold the heat vaporizes both the carbon and the liquid, so that bubbles are formed. These appear on longer time scales, as reported in Ref. 16, and can cause problems for high-energy or high-repetition-rate limiting applications. The disappearance of the limiting effect after multiple-pulse irradiation of a single site (before the liquid can be replenished) also confirms that the carbon particles are destroyed, i.e., in this case they are ionized and vaporized, or atomized, so that they no longer effectively scatter light.

The fluence dependence was confirmed by focal-spot-size-dependence measurements with collimated beams and by pulse-width-dependence measurements with nanosecond and picosecond irradiation. However, we showed that for a tight-focusing geometry for which the depth of focus is shorter than the sample thickness, the fluence dependence is masked, and the response becomes energy dependent (i.e., independent of focusing). This is an important consideration in optical-limiting applications.

The process involved in a CBS is commonly referred to as laser-induced damage, and we have prepared a material with a low damage threshold. Our understanding of the limiting mechanisms also tells us that we will not be able to lower the limiting threshold significantly (i.e., by 10×) or increase the bandwidth. The reasons are that the carbon is black and therefore broadband and highly absorbing. To lower the threshold we must either increase the absorptance (we cannot do this to any significant degree) or lower the ionization threshold (flooding the suspension with ionization radiation may do this). At

the moment, a carbon-black suspension is one of the most effective optical-limiting materials available for nanosecond laser pulses.

ACKNOWLEDGMENTS

We gratefully acknowledge support from the Defense Advanced Research Projects Agency, Center for Night Vision and Electro-Optics, and the Florida High Technology and Industrial Council. We thank Ken McEwan, Royal Signals and Radar Establishment (UK), and A. Miller for useful discussions.

*Present address, Jet Propulsion Laboratory, California Institute of Technology, Mail Stop 67-201, 4800 Oak Grove Drive, Pasadena, California 91109.

REFERENCES

1. K. Mansour, E. W. Van Stryland, and M. J. Soileau, Proc. Soc. Photo-Opt. Instrum. Eng. **1105,** 91 (1989).
2. K. Mansour, E. W. Van Stryland, and M. J. Soileau, Proc. Soc. Photo-Opt. Instrum. Eng. **1307,** 350 (1990).
3. W. E. Williams, M. J. Soileau, and E. W. Van Stryland, Opt. Commun. **50,** 256 (1984).
4. K. Mansour, Ph.D. dissertation (University of North Texas, Denton, Tex., 1990).
5. M. J. Soileau, W. E. Williams, and E. W. Van Stryland, IEEE J. Quantum Electron. **QE-19,** 731 (1983).
6. K. C. Jungling and O. L. Gaddy, IEEE J. Quantum Electron. **QE-7,** 97 (1973).
7. T. B. Boggess, Jr., A. L. Smirl, S. C. Moss, I. W. Boyd, and E. W. Van Stryland, IEEE J. Quantum Electron. **QE-21,** 488 (1985).
8. M. Sheik-Bahae, A. A. Said, T. H. Wie, D. J. Hagen, and E. W. Van Stryland, IEEE J. Quantum Electron. **26,** 760 (1990).
9. J. H. Marburger, *Progress in Quantum Electronics* (Pergamon, London, 1977), pp. 35–110.
10. C. N. K. Patel and A. C. Tam, Rev. Modern Phys. **53,** 517 (1981).
11. Y. P. Raizer, Sov. Phys. Usp. **8,** 650 (1966); also see F. Docchio and C. Sacchi, Invest. Ophthalmol. Vis. Sci. **29,** 437 (1986).
12. R. G. Meyerand, Jr., and A. F. Haught, Phys. Rev. Lett. **13,** 7 (1964); also see F. Docchio, P. Regondi, M. R. C. Capon, and J. Mellerio, Appl. Opt. **27,** 3669 (1988).
13. C. D. David, Jr., J. Appl. Lett. **11,** 394 (1967).
14. J. F. Ready, *Effects of High-Power Laser Radiation* (Academic Press, New York, 1971).
15. A. Vogel, W. Lauterborn, and R. Timm, J. Fluid Mech. **206,** 299 (1989).
16. K. M. Nashold, R. A. Brown, D. P. Walter, and R. C. Honey, Proc. Soc. Photo-Opt. Instrum. Eng. **1105,** 78 (1989).
17. C. G. Morgan, Rep. Progr. Phys. **38,** 621 (1976).
18. T. P. Ackerman and O. B. Toon, Appl. Opt. **20,** 3661 (1981).
19. J. B. Donnet and A. Voet, *Carbon Black Physics, Chemistry and Elastomer Reinforcement* (Dekker, New York, 1976).
20. C. D. David, Jr., J. Appl. Phys. **40,** 3674 (1969).